Preparation and Thermal Conductivity of Novolac/Ni/Graphite Nanosheet Composites

Shasha Li, Shuhua Qi, Nailiang Liu, Peng Cao, Yi Zhang

Department of Applied Chemistry, School of Science, Northwestern Polytechnical University, Xi'an 710072, China

Received 19 May 2011; accepted 20 July 2011
DOI 10.1002/app.35436
Published online 1 December 2011 in Wiley Online Library (wileyonlinelibrary.com).

ABSTRACT: A high thermal conductivity novolac/nickel/graphite nanosheet (novolac/Ni/NanoG) composite was synthesized through *in situ* polymerization. Graphite nanosheet (NanoG) was prepared by sonicating expanded graphite (EG) in an aqueous alcohol solution and was plated with nickel through an electrodeposition method. The X-ray diffraction spectrum shows that nickel was successfully plated onto the graphite surface and the nickel thickness is about 27.89 nm. The microstructures of the Ni/NanoG were characterized by scanning electron microscopy and transmission electron microscopy. The results reveal that nickel particles with the average diameter of 25 nm are coated on NanoG surface homogeneously and densely. Energy dispersive spectrometry spectrum confirms that the Ni content coated on NanoG surface, whose atomic percentage is 61%, is much higher than that of C element. The values predicted by theoretical model were underestimated the thermal conductivity of novolac/Ni/NanoG composites. Among NG, EG, NanoG, and Ni/NanoG four kinds of particles, the Ni/NanoG improved the thermal conductivity of novolac resin significantly. © 2011 Wiley Periodicals, Inc. J Appl Polym Sci 124: 4403–4408, 2012

Key words: graphite nanosheet; nickel plating; novolac resin; microscopy; thermal conductivity

INTRODUCTION

High thermal conductivity materials play an important role in electronic packing.[1] To satisfy requirements in heat dissipation, filled polymers are widely used in electronic packaging for device encapsulation owing to high thermal conductivity, chemical inertness, being light weight, and reliability against fracture to transfer high degrees of heat.[2,3] Metal and ceramic fillers are used in polymers to increase the thermal conductivity of the resultant composite. Current interest in improving the thermal conductivity of polymers is focused on the selective addition of nanofillers with high thermal conductivity.[4]

Theoretically, graphite has an extremely high thermal conductivity in the direction parallel to the graphite layers owing to its well-arrayed structures.[5] Natural graphite flake (NG) is a perfect precursor material because of its high thermal conductivity (704 W/mK) caused by a high degree of graphitization and preferential crystalline orientation.[6] Because graphite nanosheet (NanoG) has higher radius to thickness ratio than that of NG, it becomes a potential thermally conductive nanocomposite. NanoG produced from crystalline graphite requires a long time and a series of subsequent high energy operations such as dewatering, drying, regrinding, and classification because its exfoliation cannot be achieved by ion exchange reaction.[7] By detonating pure trinitrotoluene in shielding gas, graphite nanosheets can be produced. New methods for graphite nanosheet production have recently emerged. NG turns into a graphite intercalation compound after acid intercalation, easily producing expanded graphite (EG). NanoG can be exfoliated from EG via ultrasonic powdering.[7] In literature, NanoG prepared from EG provides excellent thermal conductivity enhancement when embedded in an epoxy matrix.[5,8] And the thermal conductivity properties of different forms of graphite have been studied with various polymer resins such as polypropylene,[9] polystyrene,[10–12] polyoxymethylene,[13] high density polythelene,[14] nylon 6,6,[15] and polyaniline[16] as well as silicone rubber,[17] and metal hydride.[18,19] However, the effect of NanoG on novolac resin thermal conductivity has seldom been studied.

Further improving the thermal conductivity of the novolac/NanoG composite is difficult, so nickel was chosen to deposit on the surface. Nickel coating on NanoG can increase not only strength, corrosion resistance but thermal conductivity by electrodeposition.[20–23] Thus, this study aims to investigate the preparation of novolac/Ni/NanoG via *in situ* polymerization as well as the thermal conductivity of the composite. NanoG and Ni-plated NanoG were

Correspondence to: S. Li (frostgirl82@126.com).
Contract grant sponsors: Shenyang Aircraft Design and Research Institute.

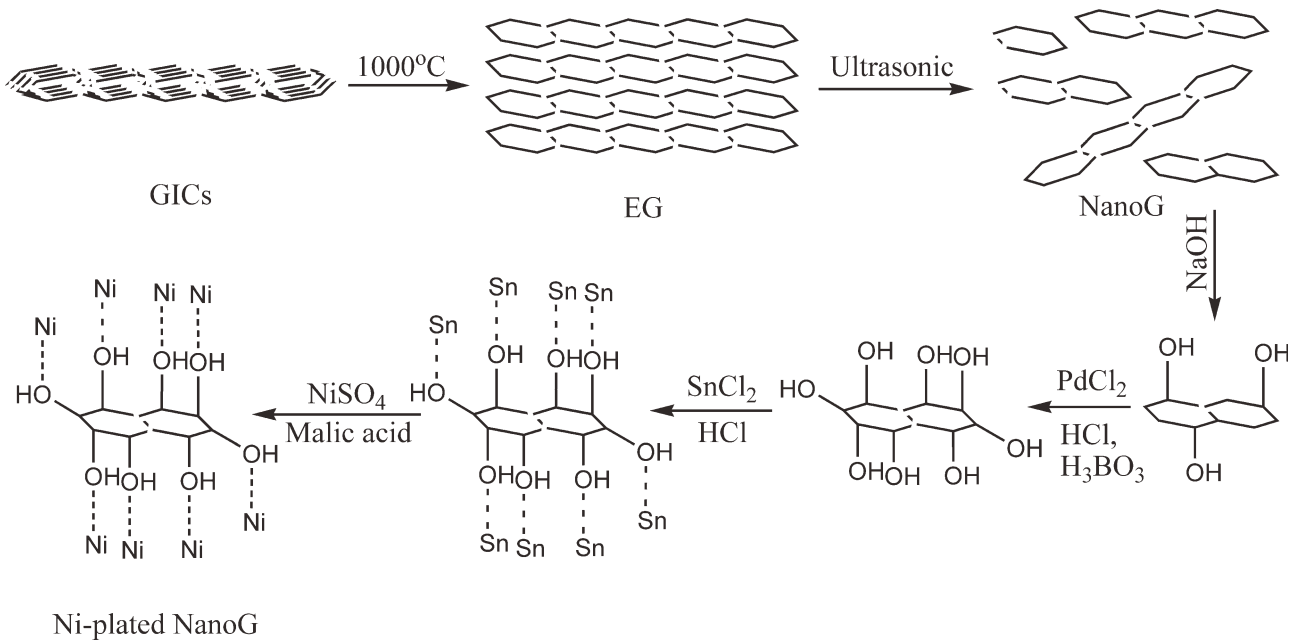

Figure 1 Process of Ni-plating NanoG.

characterized by X-ray diffraction (XRD), scanning electron microscopy (SEM), transmission electron microscopy (TEM), and energy dispersive spectrometer (EDS). The thermal conductivity of novolac/NG, novolac/EG, novolac/NanoG, and novolac/Ni/NanoG composites were also investigated.

EXPERIMENTAL

Materials

Phenol and formaldehyde (in 37 wt % water solution) were obtained from the Tianjin Damao Chemical Reagent Plant (China). Graphite intercalation compounds (GICs) were supplied by Shandong Qingdao Graphite Company (China). Thirty-six percent Hydrochloric acid (HCl), sodium hydroxide (NaOH), stannous chloride ($SnCl_2$), palladium dichloride ($PdCl_2$), boric acid (H_3BO_3), nickel sulfate ($NiSO_4$), malic acid, and alcohol, all of which were of analytical reagent grade, were provided by Shanghai Dafeng Chemical Industry (China).

Preparation of NanoG

The GICs were heated at 1000°C for 15 s in a muffle furnace to obtain EG. NanoG was prepared according to literature.[7] EG (1 g) was immersed in 400 mL aqueous alcohol solution (70 vol % alcohol and 30 vol % distilled water), then the mixture was subjected to 12 h powdering in an ultrasonic bath with a power of 100 W. The resulting dispersion was then filtered, repeatedly washed with distilled water, and dried in a thermostatic vacuum oven at 100°C to obtain NanoG. The treatment process is illustrated in Figure 1.

Preparation of Ni-plated NanoG

Preparation of Ni-plated NanoG consists of oxidation, sensitization, activation, and rinsing. First, NanoG powder was oxidized in 40 g/L NaOH solution at 40°C for 2 h. After rinsing with distilled water, the powder was treated with a solution [50 g/L $PdCl_2$, 20 g/L H_3BO_3, and 2 mL/L HCl] at room temperature for 0.5 h. The NanoG powder was rinsed and mixed with 10 g/L $SnCl_2$ and 20 mL/L HCl aqueous solution at 60°C for 0.5 h. The treated NanoG powder was rinsed with distilled water until its pH value reached about 7. Subsequently, 50 g/L malic acid and 10 g/L $NiSO_4$ were added simultaneously into the pretreated NanoG ethanol aqueous solution, with continuous stirring at 60°C for 1 h (Fig. 1). Ni-plated NanoG was finally obtained after washing with distilled water and drying in a vacuum at 100°C.

Preparation of composites

In a 250 mL three-necked round bottom flask equipped with a stirrer, thermometer, and condenser, 96 g phenol, 70.5 g formaldehyde, and 0.1 g hydrochloric acid were respectively combined with NG, EG, NanoG, and Ni-plated NanoG to produce different composites. The reaction mixtures were kept at 80°C for 4 h. After adjusting pH and reducing pressure distillation, each mixture was quickly injected into a sealed glass mold coated with mold

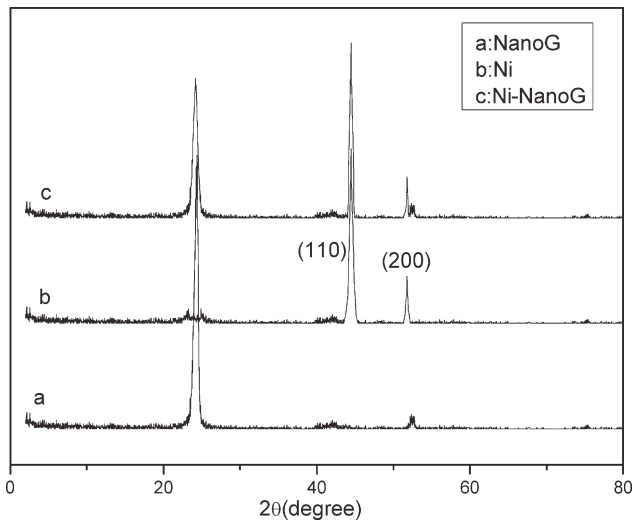

Figure 2 XRD of NanoG and Ni-plated NanoG.

release agent. The mold was placed in a vacuum drying oven set at 0.08 MPa at 170°C for 1 h. After cooling to room temperature, the four composites were molded.

Characterization

XRD characterization was performed using an XRD-6000 instrument (SHIMADZU, Japan) at a scan rate of 0.02° with Cu-$K\alpha_1$ radiation generated at a voltage of 40 kV and a current of 40 mA. The X-ray patterns for 2θ from 10°–80° were obtained.

Morphological analysis was performed using a JSM-6390 LV SEM (JEOL, Japan) and a JSM-3010 TEM (JEOL, Japan) with an energy dispersive X-ray spectroscopy (EDS) instrument. Observations were carried out to examine the microstructure of graphite in every step of the procedure and the element concentration in Ni-plated NanoG.

The thermal conductivity of the composites was tested using a LFA 457 thermal analyzer (NETZSCH, Germany). Testing was based on the well-established flash method widely used in testing the thermal properties of solid materials after decades of continuous improvement. The measurement principle is as follows: The front side of a plane parallel solid sample is heated by a short laser pulse. The absorbed heat induced propagates through the sample and causes a temperature increase on the rear surface. The temperature rise is measured versus time using an infrared detector. The thermal conductivity is determined by the equation

$$\lambda(T) = a(T) \cdot cp(T) \cdot \rho(T) \quad (1)$$

where λ is thermal conductivity, a is thermal diffusivity, c_p is in most cases specific heat, and ρ is density.[24]

RESULTS AND DISCUSSION

XRD analysis of Ni-plated NanoG

To learn the Ni coating thickness on the surface of NanoG, Ni-plated NanoG was examined via XRD spectrum. Figure 2 shows the XRD spectra of NanoG, Ni, and Ni-plated NanoG. The typical graphite pattern can be seen in Figure 2(a); the two diffraction peaks correspond to planes (002) and (110) in graphite. Figure 2(c) shows the graphite diffraction peak and three diffraction peaks of the typical nickel pattern corresponding to planes (111), (200), and (220) in Ni [Fig. 2(b)]. The peak intensity of graphite in Figure 2(c) is significantly weaker than that in Figure 2(a); whereas the peak intensity of Ni is much stronger than that of graphite. This indicates that the NanoG surface has been almost completely coated by Ni. According to the Debye-Scherrer equation

$$D = K\lambda/\beta\cos\theta \quad (2)$$

where D is average crystallite size, K is the sharp factor which is 0.9 for reception, λ is the X-ray wavelength, β is the full-width of half-maximum of the peak, and θ is the diffraction angle. XRD data shows that the thickness of the Ni-plated NanoG is about 46.39 nm and that of NanoG is around 18.5 nm. Therefore, the Ni coating thickness is about 27.89 nm.

Microscopy of GICs, EG, NanoG, and Ni-plated NanoG

The microscopy results of GICs, EG, NanoG, and Ni-plated NanoG are shown in Figure 3. The GICs sheets have irregular lamellar shapes ~500 μm in diameter and 3–16 μm in thickness. Every GICs sheet consists of thousands of thinner sheets. The microscopy of a GICs sheet is shown in Figure 3(a). There are different distances between each GICs sheet; indicating that many compounds can expand to stretch the GICs sheets during heat treatment to form EG.

The structure of EG is looser, more porous, and worm-like because of the nonuniform distribution of compounds. Generally, EG volume is 800 times that of its predecessor, GICs.[25] From Figure 3(b), the microstructure of EG appears to be a crisscross network of thin sheets. Seen another way, one GICs appears to be split into thousands of smaller pieces without separating completely. Furthermore, the smaller pieces are thin enough to make the other pieces underneath visible.

The high energy generated by ultrasonic wave induces high-velocity interparticle collisions and causes fragmentation of NanoG. The SEM images of NanoG are presented in Figure 3(c). Small graphite

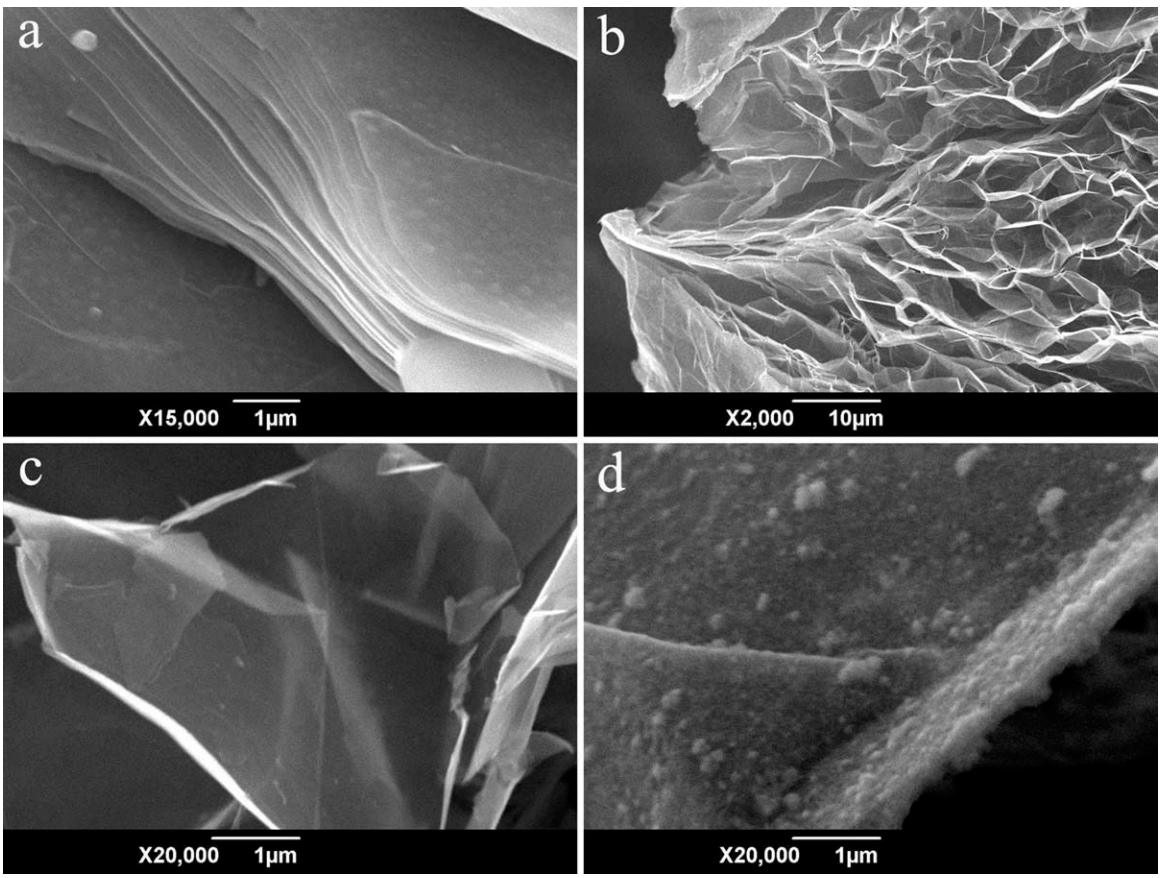

Figure 3 SEM of GICs, EG, NanoG, and Ni-plated NanoG.

pieces separate from EG and became almost transparent NanoG. NanoG is highly disordered with curls and has a diameter of 5–10 μm and a thickness of 10–100 nm, indicating a large radius-thickness ratio. The contact surface area of NanoG is therefore larger than that of GICs under the same quantity.

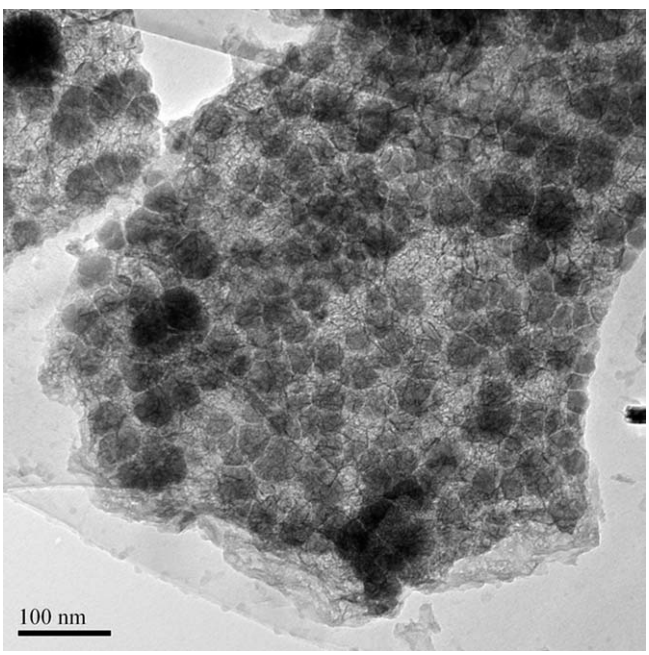

Figure 4 TEM of Ni-plated NanoG.

Ni plating on the NanoG surface can effectively increase the thermal conductivity of the composite because of the good thermal conductivity of Ni. From Figure 3(d), Ni particles have been coated onto the NanoG surface like a film. These particles are homogeneous and dense; some Ni particles gather to form aggregates on the Ni film surface. The overall thickness of the Ni-plated NanoG from Figure 3(d) is about 214 nm. The thickness obtained is greater than the XRD results because the viewing angles may have been different and all NanoG sheets possibly did not share the same thickness.

The TEM image of the Ni-plated NanoG is shown in Figure 4. NanoG is almost completely covered by Ni particles, like many balls crowding together. Several bigger particle aggregates come from small particles, showing darker areas than others. The average diameter of the Ni particles is around 25 nm, indicating that the average thickness of Ni coating is about 25 nm.

The EDS spectrum (Fig. 5) of Ni-plated NanoG confirms that the surface of NanoG is coated by Ni. Ni element content, whose atomic percentage is 61%, is much higher than that of C (22%), so does its weight percentage. The Ni weight percentage is 87.1%, while that of C is only 6.4%.

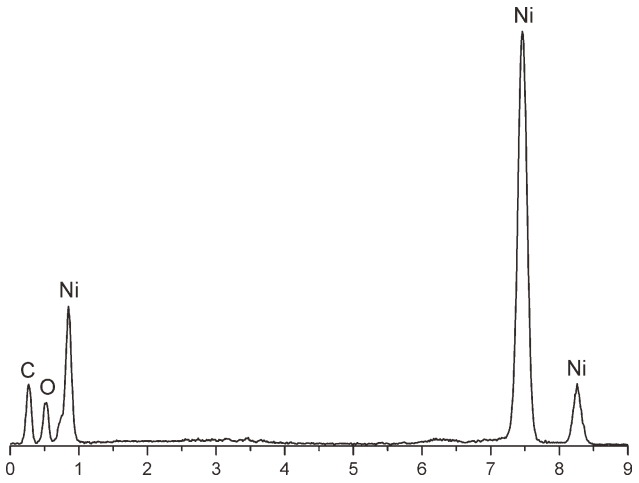

Figure 5 EDS of Ni-plated NanoG.

Composite thermal conductivity models

The thermal conductivity of graphite (704 W/mK) is more than 6000 times that of novolac resin (0.11 W/mK). The graphite particle affects the thermal conductivity as shown in Figure 6. The thermal conductivity increased with increasing filler concentration.

Various theoretical models on the thermal conductivity of composites have been published to predict the thermal conductivity of composites as a function of fillers. Maxwell-Eucken, Bruggeman, Nielsen-Lewsi, and Russell models have been used to evaluate the thermal conductivity of composites.[3,26–28]

The Maxwell equation takes into account the particle volume concentration and thermal conductivities of the particle and the liquid.[26] The thermal conductive particles of the composite prepared by a homogeneous sphere without random interaction are dispersed in the matrix. The Maxwell–Eucken model can be predicted by

$$\lambda = \lambda r \frac{[2\lambda r + \lambda p + 2Vp(\lambda p - \lambda r)]}{[2\lambda r + \lambda p - Vp(\lambda p - \lambda r)]} \tag{3}$$

whereλ, λ_r, and λ_p are the thermal conductivity of the composite, resin, and particle, respectively; V_p is the volume fraction of the particle.

The Bruggeman model shows an implicit relationship between the thermal conductivities of the composite, the filler, and the matrix for dispersion. It can be explained by

$$1 - Vp = \frac{(\lambda p - \lambda)(\lambda r/\lambda)^{1/3}}{(\lambda p - \lambda r)} \tag{4}$$

where λ, λ_r, and λ_p are the thermal conductivity of the composite, resin, and particle, respectively; V_p is the volume fraction of the particle.

On the other hand, the Nielsen–Lewsi model considers the particle shape, aggregate type, and orientation style in the matrix. It can be shown by

$$\lambda = \lambda r \frac{1 + ABVp}{1 - \psi BVp},$$

where

$$B = \frac{\frac{\lambda p}{\lambda r} - 1}{\frac{\lambda p}{\lambda r} + A}, \psi = 1 + \left(\frac{1 - \phi r}{\phi r^2}\right) Vp \tag{5}$$

where λ, λ_r, and λ_p are the thermal conductivity of the composite, resin, and particle, respectively; V_p is the volume fraction of the particle; and ϕ_r is the maximum accumulation volume fraction of the dispersed particle. The values of A and ϕ_r are chosen as 3 and 0.637.

The Russell model assumes that the dispersed phase is a cube, which has the same size and no interaction in the matrix. It can be defined by

$$\lambda = \lambda r \left[\frac{Vp^{2/3} + \frac{\lambda r}{\lambda p}(1 - Vp^{2/3})}{Vp^{2/3} - Vp + \frac{\lambda r}{\lambda p}(1 + Vp - Vp^{2/3})}\right] \tag{6}$$

where λ, λ_r, and λ_p are the thermal conductivity of the composite, resin, and particle, respectively; V_p is the volume fraction of the particle. However, particle size has not been accounted for in any of the classical models.[26]

The experimental values of the novolac/Ni/NanoG thermal conductivity are shown in Figure 6. When filler concentration reaches 60 wt %, thermal conductivity increases to 0.806, more than 7 times that of pure resin. This rapid growth may be attributed to the significant conductive pathways formed in the composite. No suitable thermal conductivity

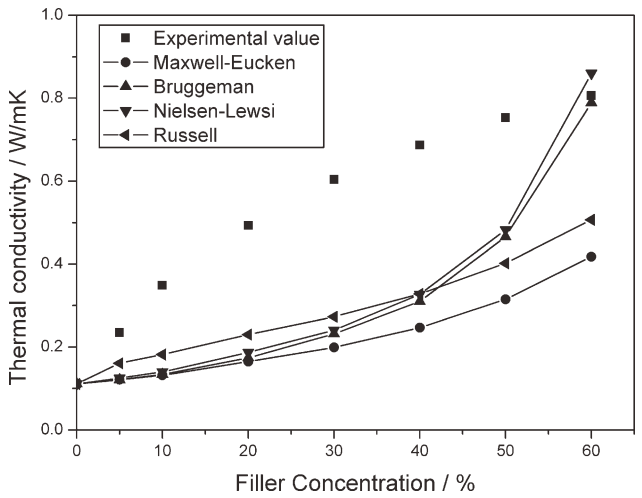

Figure 6 Thermal conductivity of the composites with different filler mass fractions.

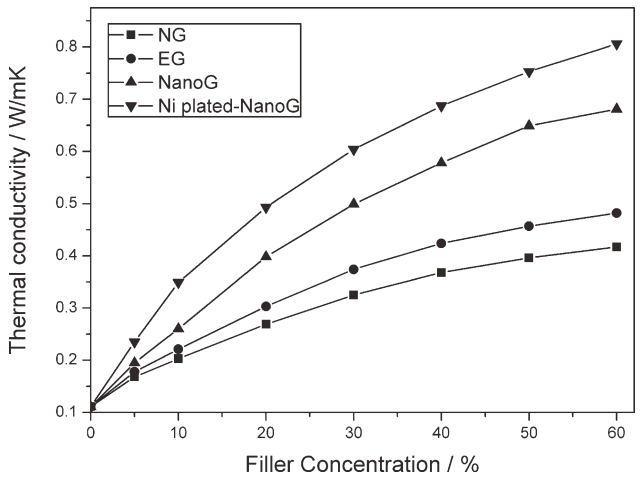

Figure 7 Different particles enhanced novolac thermal conductivity.

model from the four classical models was apparent. This is mainly because the NanoG sheets in the composites have irregular shapes, different sizes, and orientation. These conditions do not fit any premise of the four classical models, so the trend differs from the models. Generally, the thermal conductivities of composites show a gradual growth trend. However, the growth rates here decrease by degree; this is because the thermal conduction pathway has been connected. There is little space to form more paths and other fillers only enhance these paths. Therefore, the growth rate no longer increases.

Thermal conductivity of different composites

Figure 7 shows that the four kinds of filler particles have different abilities of increasing novolac resin thermal conductivity. NG has the highest density among these fillers. At the same concentration, it took up the smallest volume fraction in the composites. Therefore, it cannot enhance thermal conductivity effectively. Though EG has a lower density than NG, the expanded spaces cannot contact with the resin completely. The spaces and reunion stop EG from increasing the thermal conductivity significantly. NanoG can strongly increase the thermal conductivity of novolac resin not only because of low density, but also own to its good dispersion in the novolac resin. After being coated by nickel, a good thermal conductor, the NanoG sheets increase thermal conductivity faster than before. Ni-plated NanoG can effectively enhance the thermal conductivity of novolac resin on all four types of graphite used.

CONCLUSIONS

A high thermal conductivity novolac/nickel/graphite nanosheet composite was prepared through *in situ* polymerization. NanoG was prepared by sonicating EG in an aqueous alcohol solution. Then, NanoG was plated with nickel through an electroless plating method. The XRD spectra show that nickel was successfully plated on the graphite surface. The microstructures of the Ni-plated NanoG were characterized by SEM and TEM. EDS spectrum confirms that the surface of NanoG is coated by Ni. The Ni content, whose atomic percentage is 61%, is much higher than that of C (22%), indicating that Ni is thicker than NanoG. The experimentally obtained thermal conductivity values did not agree with the predicted data from any of the four classical thermal conductivity models. Among NG, EG, NanoG, and Ni-plated NanoG, Ni-plated NanoG most significantly improved the thermal conductivity of novolac resin. The thermal conductivity of novolac/Ni/NanoG composite is 0.806, more than 7 times that of pure novolac resin.

The authors are thankful to the companies and relatives who kindly offered materials and help.

References

1. Rimdusit, S.; Ishida, H. Polym Compos 2000, 41, 7941.
2. Pezzotti, G.; Kamada, I.; Miki, S. J Eur Ceram Soc 2000, 20, 1197.
3. Wong, C. P.; Bollampally, R. S. J Appl Polym Sci 1999, 74, 3396.
4. Han, Z.; Fina, A. Prog Polym Sci 2011, 36, 914.
5. Yu, A.; Ramesh, P.; Itkis, M. E.; Bekyarova, E.; Haddon, R. C. J Phys Chem 2007, 111, 7565.
6. Liu, Z.; Guo, Q.; Shi, J.; Zhai, G.; Liu, L. Carbon 2008, 46, 414.
7. Chen, G.; Weng, W.; Wu, D.; Wu, C.; Lu, J.; Wang, P.; Chen, X. Carbon 2004, 24, 753.
8. Ganguli, S.; Roy, A. K.; Anderson, D. P. Carbon 2008, 46, 806.
9. Wakabayashi, K.; Brunner, P. J.; Masuda, J.; Hewlett, S. A. Polymer 2010, 51, 5525.
10. Xiao, M.; Sun, L.; Liu, J.; Li, Y.; Gong, K. Polymer 2002, 43, 2245.
11. Zou, J.; Yu, Z.; Pan, Y.; Fang, X.; Ou, Y. J Polym Sci Part B: Polym Phys 2002, 40, 954.
12. Tu, H.; Ye, L. Polym Adv Technol 2009, 20, 21.
13. Zhao, X.; Ye, L. J Appl Polym Sci 2009, 111, 759.
14. Ye, C.; Shentu, B.; Weng, Z. J Appl Polym Sci 2006, 101 3806.
15. Weber, E. H.; Clingerman, M. L.; King, J. A. J Appl Polym Sci 2002, 88, 123.
16. Wu, X.; Qi, S.; He, J.; Chen, B.; Duan, G. J Polym Res 2009, 17, 751.
17. Mu, Q.; Feng, S. Thermochim Acta 2007, 462, 70.
18. Kima, K. J.; Montoya, B.; Razania, A.; Lee, K. H. Int J Hydrogen Energy 2001, 26, 609.
19. Sanchez, A. R.; Klein, H. P.; Groll, M. Int J Hydrogen Energy 2003, 28, 515.
20. Palaniappa, M.; Babu, G. V.; Balasubramanian, K. Mater Sci Eng A 2007, 471, 165.
21. Li, L.; An, M. J Alloys Compd 2008, 461, 85.
22. Lee, C. K. Surf Coat Technol 2008, 202, 4868.
23. Tang, X.; Cao, M.; Bi, C.; Yan, L.; Zhang, B. Mater Lett 2008, 62, 1089.
24. Selin, M.; König, M. Metall Mater Trans A 2009, 40, 3235.
25. Kim, S.; Drzal, L. T. Sol Energy Mater Sol Cells 2009, 93, 136.
26. Yu, W.; Choi, S.U.S. J Nanopart Res 2003, 5, 167.
27. Keith, J. M.; King, J. A.; Lenhart, K. M.; Zimny, B. J Appl Polym Sci 2007, 105, 3309.
28. Progelhof, R. C.; Throne, J. L.; Ruetsch, R. R. Polym Eng Sci 1976, 16, 615.